

Proton channels govern vesicular carbonate chemistry in mineralizing cells of a marine calcifier

Received: 20 March 2025

Accepted: 6 March 2026

Published online: 18 March 2026

 Check for updates

Sima Jonusaite^{1,2}, Catrin Przibylla-Diop¹, Marianne Musinszki¹, Ornina Merza¹, Marcus Schewe¹, Thomas Baukrowitz¹ & Marian Y. Hu¹✉

Biom mineralization shapes the geology of our planet and is an integral part of the global carbon cycle. Many calcifying organisms generate biomineral precursors within their cells but the mechanisms controlling carbonate chemistry in the calcifying vesicles remain unknown. Using the sea urchin embryo that is a prime model for biomineralization by intracellular amorphous calcium carbonate (ACC) formation this work demonstrated a high proton permeability of the calcifying cells and their vesicles. Intra-vesicular pH and Ca²⁺ recordings demonstrate highly alkaline conditions in ACC forming endocytotic Ca²⁺-rich vesicles, that are enriched during the mineralization process. Using confocal live-cell imaging we observe how vesicles exocytose their Ca²⁺-rich and alkaline contents to the calcification front. We identify the proton channel Otop2l as a master regulator for membrane proton conductance in calcifying cells, using the membrane potential to control pH conditions at the site of mineral precursor formation. Electrophysiological investigations demonstrate that Otop2l is activated by alkaline conditions as well as Mg²⁺ and Ca²⁺ ions. We provide evidence for high intracellular proton conductance as mechanism to generate alkaline pH conditions in the calcification vesicles. This deep mechanistic knowledge can help explain sensitivities of marine calcifiers to rapid changes in seawater pH in past and future marine habitats.

The process of mineralization in animals and plants has led to the emergence of biogenic structures like chalk mountains and barrier reefs that shape the surface of our planet and thereby have profound impacts on the global carbon cycle. The generation of CaCO₃ by marine organisms has evolved in the world's oceans under very stable conditions with respect to the seawater carbonate system and pH over long geological timescales¹. CaCO₃ production in biological systems has been demonstrated to strongly depend on the availability and uptake of calcium from the environment^{2–4}, while carbonate species can be derived from the environment or internal metabolic sources^{5,6}. The calcium carbonate saturation state (Ω) is a function of the pH, with alkaline conditions shifting the equilibrium towards the CO₃²⁻ side,

while acidic conditions favor the formation of CO₂. Therefore, pH is a master regulator of the carbonate system and under current oceanic conditions of pH-8.1 causes an oversaturation of carbonate species ($\Omega > 1$), thermodynamically favoring calcification. Importantly, a decrease in seawater pH due to increasing atmospheric pCO₂, termed as ocean acidification (OA), has been demonstrated to represent a major factor that can negatively impact marine calcifying organisms^{7–10}.

A large body of knowledge has been generated regarding trans-epithelial and cellular mechanisms that promote transport of ions and regulation of pH critical for the formation and stabilization of CaCO₃ skeletons in marine organisms². These mechanisms can generate high

¹Institute of Physiology, Kiel University, Kiel, Germany. ²Department of Biological Science, University of Tulsa, Tulsa, OK, USA.

✉ e-mail: m.hu@physiologie.uni-kiel.de

calcite (Ω_{cal}) and aragonite (Ω_{Ar}) saturation states at the mineralization front that, together with matrix proteins, promote crystal formation and protect from dissolution even under decreased environmental pH and carbonate saturation states^{11–13}. Mounting evidence demonstrates that, besides the regulation of carbonate chemistry at the calcification front outside of calcifying cells, intracellular formation of metastable calcification precursors (i.e., amorphous calcium carbonate; ACC) within specialized vesicles is an initial step in the mineralization process of major marine calcifiers, including corals^{14,15}, molluscs¹⁶, and echinoderms¹⁷. However, the abiotic conditions in these calcifying vesicles and the regulatory mechanisms that control pH and carbonate chemistry in these subcellular compartments remain enigmatic.

Currently, the sea urchin larva with its calcitic endoskeleton represents one of the best-studied models for the vesicular formation of ACC by the calcifying primary mesenchyme cells (PMCs)^{17–20}. The sea urchin larva has a highly permeable ectoderm that surrounds the body cavity filled with a proteoglycan matrix and seawater-like fluids²¹. All cells and tissues, including the gut and the PMCs, are embedded in this matrix and thereby directly experience changes in environmental pH. The current model denotes that PMCs endocytose seawater-like fluids from the extracellular space of the primary body cavity into large (up to 1 μm diameter) vesicles that split into a number of smaller vesicles in which ACC is formed²². An X-ray absorption near-edge structure (XANES) spectrum of individual PMC vesicles demonstrated a continuum of ACC hydration states from highly disordered states of $\text{ACC} \times \text{H}_2\text{O}$ to anhydrous ACC¹⁹. These different states of ACC formation were underlined by a very wide range of total vesicular Ca^{2+} concentrations ranging from 1 to 15 M¹⁹. Analyses using a novel scanning electron microscopy (correlative airSEMTM) demonstrated a colocalization of high vesicular calcium with calcein, a fluorescent dye that exhibits bright green fluorescence upon binding to free Ca^{2+} ²³. While these observations explain the route of Ca^{2+} transport to the site of calcification, the mechanism of dissolved inorganic carbon (DIC) accumulation remains less well understood. Earlier studies demonstrated that in the sea urchin embryo, 60% of the carbon deposited into the skeleton is derived from metabolic CO_2 , while the remaining 40% is absorbed from the seawater⁶. The mechanism of DIC uptake into PMCs points to a Na^+ -dependent HCO_3^- co-transporter (Sp_Slc4a10) which acts in concert with the extracellular carbonic anhydrase Cara7 to enrich the intracellular DIC pool from external HCO_3^- as well as metabolic CO_2 ^{24,25}. However, the pathway of vesicular carbon concentration and its coupling to pH regulatory features of these subcellular compartments are currently not understood.

A major physiological challenge imposed on the cell by the generation of CaCO_3 from HCO_3^- or even CO_2 lies in the liberation of protons (H^+) that need to be removed from the site of calcification (i.e., lumen of vesicles) to maintain a high carbonate saturation state and to protect cellular function. In theory, for the sea urchin larva that uses 40% of DIC (i.e., HCO_3^-) derived from seawater and 60% from metabolic CO_2 , 1.6 mol of H^+ will be liberated for each mole of CaCO_3 precipitated⁶. Thus, removal of H^+ from the site of mineral formation is a key requisite of any calcifying system^{8,26}. Despite their importance in the calcification process, H^+ transport pathways have been relatively little studied in marine calcifying systems. In the cocolithophore *Emiliania huxleyi*, an Hv1 H^+ channel has been proposed to export H^+ from the cell^{9,27}. Recently, the H^+ channel Otopetrin 2-like (Otop2l) has been identified to be a critical player for the removal of H^+ liberated by the intracellular calcification process in PMCs of the sea urchin larva⁸. Otopetrins represent a novel family of H^+ -selective channels that are essential for the formation of CaCO_3 structures in vertebrates, including statoconia and otoliths^{28–30}. Unlike Hv1 H^+ channels, otopetrins are not voltage-gated but instead display a characteristic pH gating^{8,28}. Knock-down of Otop2l in the sea urchin larva led to skeletal defects and reduced permeability of the PMC plasma membrane to H^+ ⁸.

The identification of H^+ channels in cocolithophores and sea urchin PMCs can explain relatively high H^+ permeability across the plasma membrane of these calcifying cells, which provides an exit for protons from the cytosol^{8,9,31}. A prerequisite for such H^+ permeability of the calcifying cell and its vesicular compartments is a tightly regulated extracellular environment. In the case of sea urchin larvae and many other marine invertebrates that lack extracellular pH (pH_e) regulatory systems, the marine environment represents their extracellular space, characterized by very stable pH conditions over long geological timescales¹.

In this study, we address the hypothesis that marine calcifiers that employ H^+ channels in their mineralizing cells are characterized by a high H^+ permeability to maintain elevated pH at the site of mineral formation. Using sea urchin larva, we identify the proton channel Otop2l as a master regulator for membrane proton conductance in the calcifying cells, where it uses the membrane potential to control pH conditions at the site of mineral precursor formation. Further electrophysiological investigations reveal the importance of seawater-associated abiotic factors affecting the activity of Otop2l. This information is essential to understand the mechanisms of intracellular ACC formation, and how the calcification process is impacted by changes in seawater pH in past, present, and future marine environments.

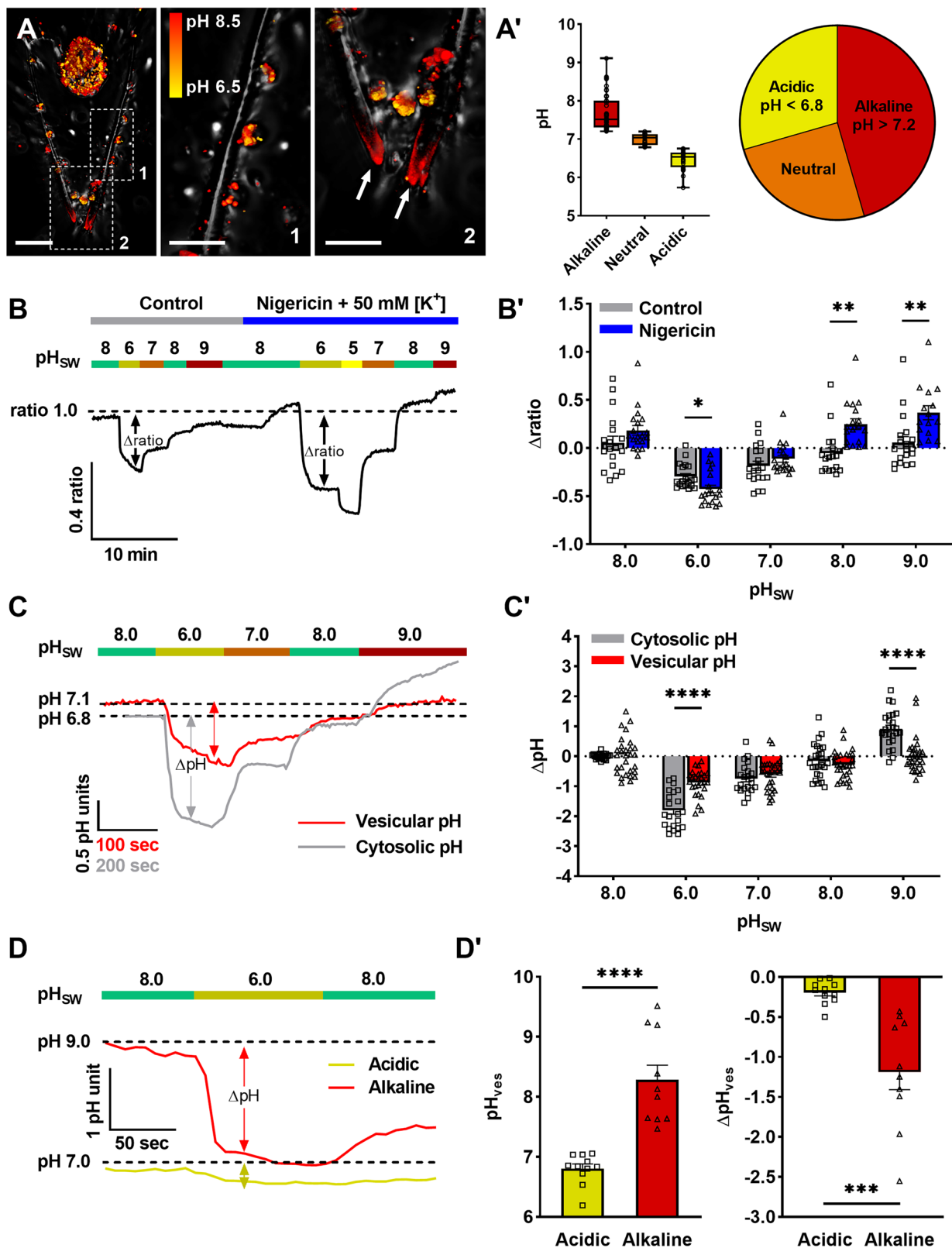
Results

Proton permeability of the plasma membrane and endocytic vesicles

To determine the pH within endocytotic vesicles of live PMCs, we used the membrane-impermeable pH-sensitive dye carboxy-SNARF. Incubation of 3–4 dpf larvae in SNARF led to an endocytotic uptake of the dye into vesicles and large vacuoles of primary mesenchyme cells (PMCs) (Fig. 1A). Large vacuoles were predominantly observed in cell bodies, whereas smaller fluorescently labeled vesicles were found throughout the syncytial cables that enclose the larval skeleton. After a longer incubation period, the dye was also incorporated into the newly built skeleton in the sheitel region that is characterized by high mineralization rates (Fig. 1A; arrows). Interestingly, SNARF dye deposited in the skeleton revealed alkaline pH ($>\text{pH } 8.0$) within the freshly formed mineral surrounded by the PMC syncytial cables (Fig. 1A). For the vesicles of PMCs, our intra-vesicular pH (pH_{ves}) measurements demonstrated a wide range of pH conditions from acidic pH <6.5 to alkaline pH >8.5 . The majority (45%) of vesicles had alkaline pH >7.2 , with the highest pH values close to the resolution limit of the dye at pH 8.5 (Fig. S1). The remaining vesicles were near-neutral or acidic, contributing 25% and 30%, respectively, to the total number of vesicles (Fig. 1A').

If the pH_{ves} is affected by H^+ permeability of the PMC, a pH change on the extracellular side should lead to a concomitant change in pH_{ves} . We therefore recorded pH_{ves} during changes in pH_e . Our measurements revealed a substantial H^+ permeability between the lumen of the vesicles and the extracellular space (Fig. 1B). Acute pH_e changes by two pH units in the perfusion solution resulted in a drop in pH_{ves} by up to 1 pH unit, whereas alkalization to pH 9 had no effect on pH_{ves} compared to control conditions at pH 8 (Fig. 1B', C, C'). Permeabilization of all membranes by the H^+/K^+ ionophore Nigericine and membrane potential (V_M) depolarization by 50 mM $[\text{K}^+]$ further enhanced H^+ permeability between the vesicles and the environment (Fig. 1B'). In general, extreme acidification down to pH 6 as well as alkaline conditions (i.e., pH 8 and pH 9) above the cytosolic pH (pH_i) led to more pronounced pH_{ves} changes in the presence of Nigericine compared to control cells that have an intact plasma V_M and controlled H^+ transport (Fig. 1B').

To further investigate the relation of PMC and vesicular H^+ permeability, we measured pH_i and pH_{ves} using membrane-permeable (cytosolic) and membrane-impermeable (vesicular) ratiometric pH-sensitive dyes. Cytosolic pH recordings during pH_e steps revealed a



high H^+ permeability of the plasma membrane that largely follows the pH_e (Fig. 1C). Measured changes in pH_i and pH_{ves} (ΔpH) during changes in ambient pH indicate lower H^+ permeability in the vesicles compared to the cytoplasm (Fig. 1C').

A detailed analysis of H^+ permeabilities in alkaline and acidic vesicles revealed a substantial drop in pH_{ves} by 1.19 ± 0.22 pH units in alkaline vesicles during a pH_e change from 8 to 6 and a drop by

0.19 ± 0.04 pH units in acidic vesicles (Fig. 1D, D'). Nevertheless, translation of the logarithmic pH scale into the actual H^+ concentration ($[H^+]$) showed a comparable H^+ permeability of both acidic and alkaline endocytotic vesicles (Fig. S2). One should note that after exposure to low pH treatment, the pH_i as well as pH_{ves} failed to recover to their initial pH when the pH_e increased back to the starting conditions of pH 8. When pH_e was raised to 9, pH_i rapidly increased back to control

Fig. 1 | Cellular and vesicular H⁺ permeability in the calcifying primary mesenchyme cells (PMCs) of the sea urchin larva. **A** Representative confocal fluorescence and bright field images of PMCs along the spicules showing luminal pH of endocytotic vesicles measured using carboxy-SNARF. Arrows point to the dye in the skeleton after longer incubation. Scale bars, 40 μ m and 20 μ m (insets). **A'** Proportion of vesicles within individual cells with alkaline ($N=51$), neutral ($N=28$), and acidic ($N=33$) pH conditions. Box plots represent median (middle line), 50% of data (box), and minima and maxima (error bars). **B, B'** Representative traces and measurements of changes in PMC vesicular pH induced by changes in external pH

in control and nigericin-treated PMCs. Values presented for individual cells as mean \pm SEM ($N=19$: controls; $N=19$: nigericin pH 8, 6, 7; $N=15$: nigericin pH 9). **C, C'** Representative traces and measurements of pH_i and pH_{ves} conditions in the PMCs during changes in pH_e. Values presented for individual cells as mean \pm SEM ($N=22$: cytosolic; $N=29$: vesicular), unpaired t -test, **** $P < 0.0001$. **D, D'** Representative traces and measurements of pH conditions in endocytotic alkaline vs. acidic vesicles during changes in pH_e. Values presented for individual cells as mean \pm SEM ($N=10$: alkaline; $N=11$: acidic), unpaired t -test, **** $P < 0.0001$, *** $P = 0.0002$.

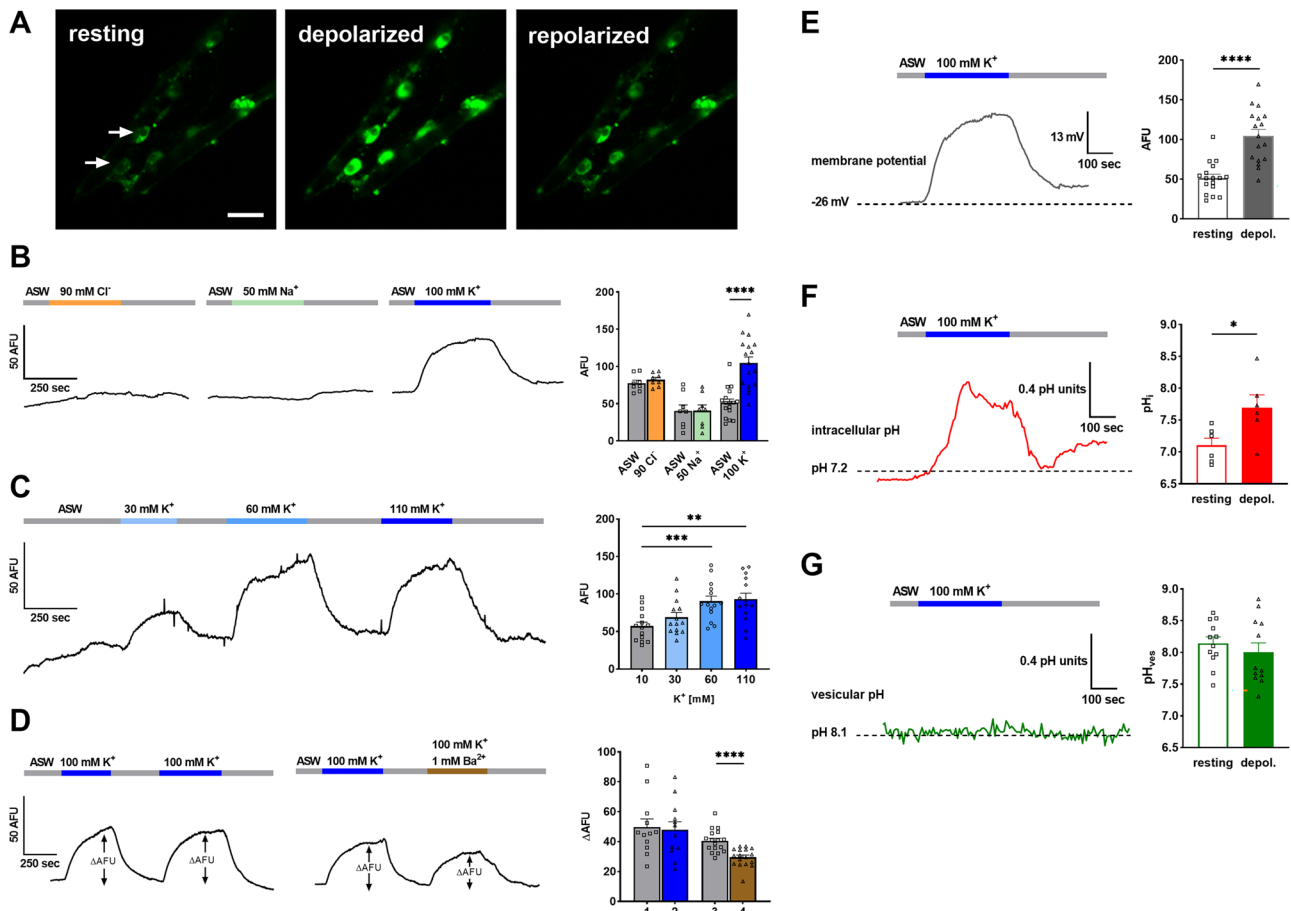


Fig. 2 | Regulation of cellular pH by V_m in the calcifying primary mesenchyme cells (PMCs) of the sea urchin larva. **A** Representative confocal fluorescence images of PMCs (arrows) containing V_m dye DIBAC₄ (green) at resting and depolarized states. Scale bar, 10 μ m. **B** Representative traces and measurements of PMC V_m intensities as artificial fluorescence units (AFUs) during changes in extracellular Cl⁻ ($N=8$), Na⁺ ($N=8$), and K⁺ ($N=17$) concentrations. Values presented for individual cells as mean \pm SEM, unpaired t -test, **** $P < 0.0001$. **C** Representative traces and measurements of PMC plasma membrane depolarization intensities by different extracellular [K⁺]. Values presented for individual cells as mean \pm SEM

($N=14$), unpaired t -test, *** $P = 0.0008$, ** $P = 0.001$. **D** Representative traces and measurements of changes in PMC plasma membrane depolarization intensity in the presence of K⁺ channel blocker Ba²⁺. Sequential measurements with 100 mM [K⁺] and 100 mM [K⁺] + Ba²⁺ ($N=12$) and 100 mM [K⁺] + Ba²⁺ ($N=17$). Values presented for individual cells as mean \pm SEM, unpaired t -test, **** $P < 0.0001$. **E–G** Representative traces and measurements of V_m , pH_i, and pH_{ves} during PMC depolarization. Values presented for individual cells as mean \pm SEM ($N=17$ for (E), 6 for (F), 12 for (G)), unpaired t -test, **** $P < 0.0001$, * $P = 0.0269$.

levels (Fig. S4). Other cells, like ectodermal cells, did not exhibit comparable H⁺ permeability, even when pH changes were translated into [H⁺] (Fig. S3).

Cellular V_m and its role in pH regulation

In most cells, a negative plasma V_m is maintained largely by K⁺ channels moving K⁺ out of the cell. A negative V_m could also help generate H⁺ gradients across the plasma membrane in the presence of a H⁺ conductance pathway. Given our observed high PMC H⁺ permeability, we next wanted to address the hypothesis that PMC V_m contributes to the

regulation of H⁺ gradients in PMCs. For the measurements of PMC V_m , we used DIBAC₄. This anionic dye emits fluorescence inside the cell and is distributed across the plasma membrane depending on the electrical potential of the plasma membrane (Fig. 2A). We found that elevating extracellular [K⁺] to 100 mM led to a significant increase in DIBAC₄ fluorescence from 51.3 ± 4.89 AFU to 104.5 ± 8.22 AFU, indicating depolarization of the PMC plasma membrane (Fig. 2B). On the other hand, changes in extracellular [Na⁺] and [Cl⁻] did not elicit any detectable changes in DIBAC₄ fluorescence, and, by extension, V_m (Fig. 2B). Exposure of PMCs to varying external K⁺ concentrations

demonstrated a $[K^+]_i$ -dependent membrane depolarization with maximum depolarization occurring at an external $[K^+]_o$ of 60 mM (Fig. 2C). Interestingly and of note, exposing the larvae to seawater with elevated $[K^+]_o$ during the phase of skeleton formation revealed reduced calcification rate (Fig. S5). We also tested the effect of 1 mM broad-band K^+ channel inhibitor Ba^{2+} on the PMC V_M and found that the extent of depolarization by high $[K^+]_o$ was significantly reduced, resulting in ΔAFU of 29.54 ± 1.48 compared to the control ΔAFU of 40.48 ± 1.85 (Fig. 2D).

Calculations of the apparent membrane potential (V_{app}) using the difference in DIBAC₄ fluorescence intensity between resting conditions and depolarization revealed a V_{app} of -26 ± 6.9 mV (Fig. 2E). Simultaneous measurements of the plasma V_M together with pH_i recordings revealed an increase in pH_i by 0.59 pH units from 7.10 ± 0.11 to 7.69 ± 0.20 during depolarization of the cell by high extracellular $[K^+]_o$ (Fig. 2F). However, in contrast to pH_i , pH_{ves} recordings during cellular depolarization did not reveal a change in pH_{ves} (Fig. 2G). These vesicles had an average pH_{ves} of 8.14 ± 0.14 under control $[K^+]_o$. On some occasions, we observed strong DIBAC₄ fluorescence in subcellular vesicles and vacuoles. We additionally used Di-8-Anepps, a fluorescent V_M sensor that emits fluorescence when integrated into the outer leaflet of the plasma membrane and increases in fluorescence upon cellular hyperpolarization. Using this dye, we observed strong fluorescence in endocytotic calcein-positive vesicles, indicative of a strong lumen-positive potential in these vesicles (Fig. S6).

Characterization of the H^+ channel Otop2l in PMCs and heterologous expression systems

Our previous discovery of Otop2l H^+ channel in the PMCs of *S. purpuratus* larva⁸ prompted us to investigate a hypothesis that, in addition to mediating H^+ conductance across the PMC plasma membrane, the channel is also important for vesicular H^+ permeability. Using our custom-made antibody against Otop2l, we confirmed its exclusive localization in the PMCs (Fig. 3A). Higher magnification images revealed Otop2l localization in the PMC plasma membrane as well as large subcellular vesicles and vacuoles (Fig. 3A'). A 3D reconstruction of Otop2l immunoreactivity in the PMCs revealed a large interconnected meshwork within PMC bodies as well as many smaller vesicles along the syncytial cables in highly calcifying regions of the spicule tips (Fig. 3B). Negative controls where the primary antibody was omitted showed no autofluorescence or unspecific binding of the secondary antibody (Fig. 3C). To determine if Otop2l is involved in the regulation of PMC pH_{ves} , we conducted pH_i and pH_{ves} measurements in combination with pH_e steps in control and Otop2l knock-down larvae. The latter experiment revealed decreased vesicular H^+ permeability in the Otop2l morphants compared to PMCs of control larvae (Fig. 3D). Here the magnitude of vesicular alkalization was significantly reduced during increases in pH_e from pH 8 to 9 in the Otop2l morphants compared to control larvae, reaching pH_{ves} of 7.1 ± 0.12 and 7.5 ± 0.09 , respectively (Fig. 3D). In addition, the rate of vesicular acidification during a pH_e change from 8.0 to 6.5 was 0.059 ± 0.009 pH units per minute in the knock-down larvae which was significantly lower compared to 0.093 ± 0.013 pH units per minute in control group (Fig. 3D). Similar to pH_{ves} , also pH_i was affected by the knock-down where Otop2l morphants displayed attenuated changes in pH_i compared to control larvae (Fig. S8). To exclude the possibility that voltage-gated H^+ channel (Hvcn1/VSOP) may also contribute to the herein observed H^+ permeability, we searched our single-cell transcriptome for the expression of this gene and found little to no expression of it along the early development of the sea urchin larva. In contrast, Otop2l is expressed highly and specifically in the PMCs in all relevant developmental stages (Fig. S7).

Given the observed effects of Otop2l knock-down on PMC pH_{ves} regulation, we further characterized its activity in heterologous expression systems. Expression of Otop2l in oocytes produced low to

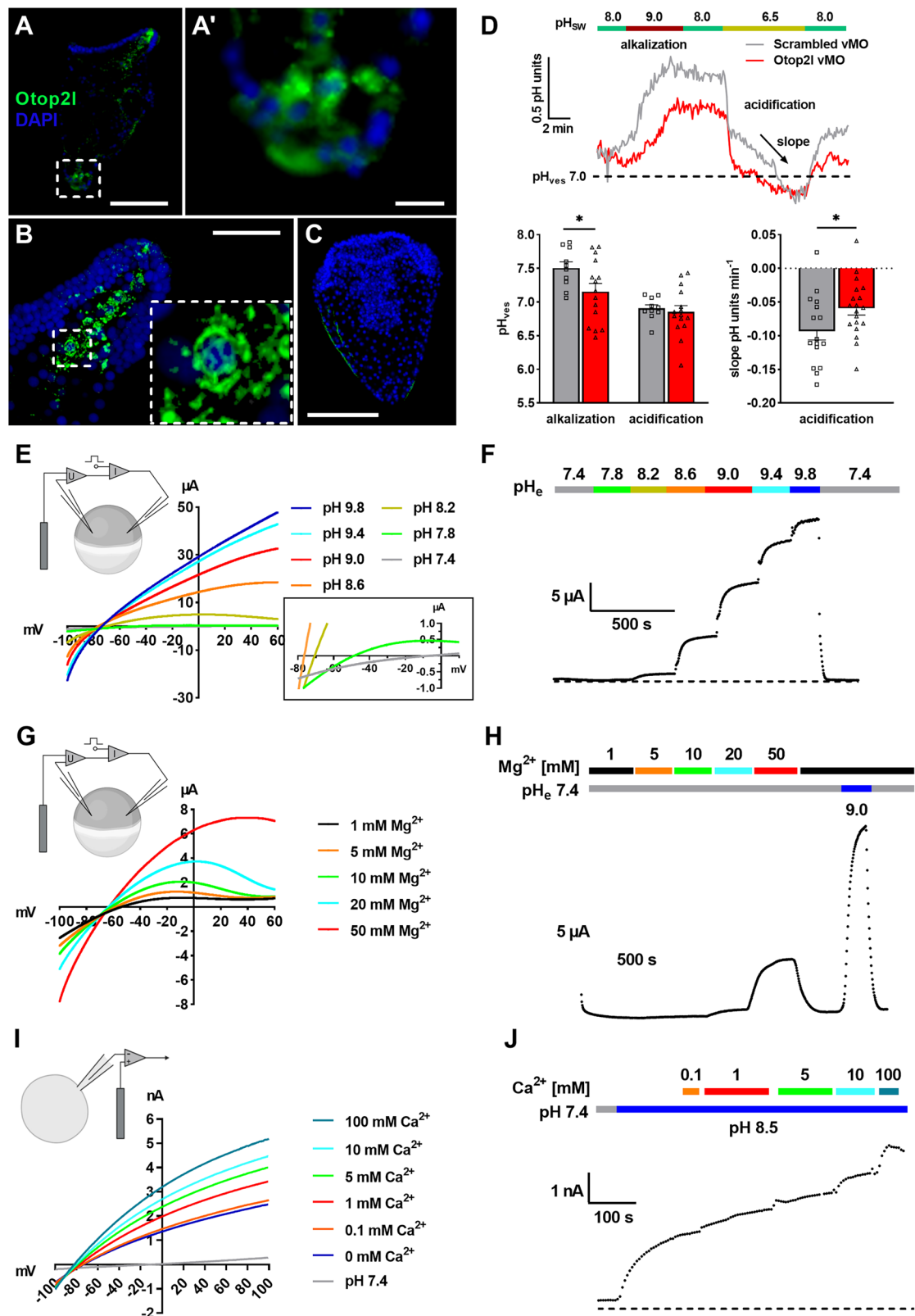
no H^+ currents at pH_e conditions < 7.8 , while elevation in pH_e up to 9.8 progressively increased H^+ currents following a sigmoidal function (Fig. 3E, F and Fig. S10A). H^+ currents ranged between 0.5 and 30 μA , depending on the pH applied on the extracellular side, with the strongest activation between pH 8.2 and pH 9.4. This demonstrates that alkaline conditions far beyond natural seawater pH (i.e., pH 7.9–8.3) stimulate the activity of this channel. In our heterologous expression experiments, we observed a shift in the reversal potential (E_{rev}) with changing pH_e conditions following the Nernst potential for H^+ (Fig. S9). Interestingly, in our oocyte experiments, the shift in E_{rev} is strongly attenuated at pH_e conditions exceeding pH 8.6. pH_i recordings in oocytes using pH-selective microelectrodes demonstrated a strong increase in pH_i at pH_e conditions > 8.6 , explaining the decreased shift in E_{rev} at these high alkaline pH conditions.

Since the seawater as well as the calcifying compartments contain high concentrations of Ca^{2+} and Mg^{2+} , we also investigated if Otop2l is further regulated by these cations. We found that in oocytes, high external Mg^{2+} also activated Otop2l currents with a low apparent affinity (EC_{50} of 31.8 ± 1.8 mM) (Fig. 3G, Fig. S10B). Remarkably, even under low pH conditions of 7.4, substantial H^+ currents of up to 7 μA were measured by the addition of 50 mM Mg^{2+} to the external bath solution (Fig. 3H). Whole-cell measurements of HEK293 cells at pH_e 8.5 showed that Ca^{2+} up to a concentration of 100 mM was able to further increase pH-preactivated Otop2l H^+ activity with a higher apparent affinity (EC_{50} of 2.97 ± 0.89 mM) than Mg^{2+} (Fig. 3I, J, Fig. S10C).

pH determination in calcein-labeled vesicles under high and low calcification activity

We used calcein labeling experiments to identify and track calcium-containing vesicles and to co-localize these with alkaline and acidic endocytotic vesicles during the calcification process. Calcein labeling performed on early pluteus larvae confirmed a rapid uptake of the dye and incorporation into the skeleton within 2–3 h (Fig. 4A). Simultaneous measurements of pH_{ves} using carboxy-SNARF demonstrated that calcein-rich vesicles partially co-localized with the pH dye (Fig. 4A', A''). From all fluorescently (calcein and SNARF) labeled vesicles, 40% contained calcein while 70% showed SNARF fluorescence (Fig. 4B). SNARF-positive vesicles were predominantly detected in the PMC cell bodies and PMC syncytium close to the skeleton (Fig. 4C, D). Within the PMC cell bodies, we observed large alkaline vacuoles with a diameter of 2–5 μm and smaller acidic vesicles. Co-localization analyses demonstrated a higher association of Ca^{2+} -rich vesicles with alkaline vesicles than with those characterized by near-neutral or acidic pH conditions (Fig. 4E). However, smaller calcein-labeled vesicles that had no SNARF labeling were frequently observed in the vicinity of larger alkaline vesicles (Fig. 4A', A''). Occasionally, we saw alkaline, calcein-positive vesicles within the syncytial cables located very close to the skeleton (Fig. 4D). 3D time-lapse recordings demonstrated highly dynamic trafficking of calcein-positive and SNARF-labeled alkaline and acidic vesicles (Movies S1, S4). On some occasions, we observed calcein-labeled and alkaline vesicles interacting very closely at the luminal membrane of the PMC syncytium, disposing their contents to the mineralization front (Movies S2, S3).

To induce high PMC calcification activity, we dissolved larval endoskeleton by incubation in seawater at pH 6, followed by transfer to a control pH where calcification is stimulated. During skeleton remineralization, the abundance of SNARF-positive endocytotic vesicles was significantly increased to 20.33 ± 1.638 vesicles per larva compared to 8.26 ± 0.879 vesicles per larva in non-re-calcifying PMCs (Fig. 4F, G). While the majority of the vesicles were alkaline vesicles in both groups, the number of neutral and acidic vesicles also increased significantly in re-calcifying PMCs compared to control larval PMCs (Fig. 4G). Strikingly, the average pH of vesicles was markedly increased from pH 8.019 ± 0.192 in non-calcifying PMCs to pH 8.511 ± 0.145 in re-calcifying PMCs (Fig. 4H, H'). Increased vesicular abundance was accompanied



by faster recovery in their pH after a low pH pulse, resulting in a change of 0.0015 ± 0.0002 pH units per second in re-calcifying PMC vesicles compared to $8.5 \times 10^{-5} \pm 0.0001$ pH units per second in non-mineralizing PMC vesicles (Fig. 4H, H'). Also, the absolute recovery in pH_{ves} was higher in the re-calcifying vesicles, while vesicles in non-mineralizing larvae failed to recover from low pH stress (Fig. 4H'). Intracellular pH recordings also demonstrated increased pH_i to

8.35 ± 0.10 in the re-calcifying PMCs compared to pH_i 7.46 ± 0.14 in non-calcifying cells and better ability of the former to recover their pH_i after a low pH pulse (Fig. 4I, I'). Despite differences in pH_i and response to low pH stress in control and re-calcifying PMCs, there was no apparent change in V_M or high K⁺ induced depolarization intensity between the two groups (Fig. 4J)

Fig. 3 | Otop2l localization and activity in calcifying primary mesenchyme cells (PMCs) and regulation by pH_e , Mg^{2+} , and Ca^{2+} . A–C Otop2l immunoreactivity was detected in the PMCs of **A**, **A'** the scheitel region, and **B** the aboral arm tips, with subcellular localization in the plasma membrane and vesicles. Larva probed with secondary antibody only shown in **(C)**. Nuclei counterstained blue with DAPI. Scale bars, 100 μm (**A**, **C**), 20 μm (**A'**, **B**). Immunostainings were repeated four times, and negative controls were performed in parallel each time. **(D)** Representative traces and measurements of PMC pH_{ves} regulation in scrambled control and vivo morpholino-mediated Otop2l knock-down larvae during alkalization and acidification stress. Values presented as mean \pm SEM ($N=10$ individual cells from six larvae (scrambled vMO) and $N=19$ from eleven larvae (Otop2l vMO)), unpaired t -test, $*P=0.0486$ for pH_{ves} , $*P=0.0436$ for acidification slope. **E** Representative

whole-cell currents of a sea urchin Otop2l expressing oocyte evoked by voltage ramps from -100 mV to $+60$ mV ($V_{\text{H}}=-80$ mV) under different external pH (pH_e) conditions ranging from near-neutral pH_e 7.4 to alkaline pH_e 9.8 ($N=27$). The inset shows the voltage ramps at pH_e 7.4, 7.8, 8.2, and 8.6. The correlation of E_{rev} and pH_e values is presented in Fig. S9. **F** Time course of Otop2l activation at $+50$ mV by increasing pH_e as measured in **(E)**. **G**, **H** Representative currents recorded and analyzed as in **(E**, **F**) for different external $[\text{Mg}^{2+}]$ conditions ($N=6$). **I** Representative whole-cell currents of a sea urchin Otop2l expressing HEK293 cell evoked by voltage ramps from -100 mV to $+100$ mV ($V_{\text{H}}=-80$ mV) under different external $[\text{Ca}^{2+}]$ conditions. **J** Time course of current activation by increasing external $[\text{Ca}^{2+}]$ as measured in **(I)** and analyzed at $+80$ mV. Created in BioRender. Hu (2026) <https://BioRender.com/aha09c2>.

Discussion

Calcifying cells have a high H^+ permeability that impacts pH_{ves}
Intra-vesicular pH recordings using membrane-impermeable fluorescent dyes that are absorbed into the cells by endocytosis demonstrated distinct pH conditions in the vesicles of PMCs. Our pH_{ves} measurements revealed that 45% of all endocytotic vesicles are alkaline, while the remaining vesicles are near-neutral or acidic, contributing 25% and 30%, respectively, to the total number of vesicles. These numbers corroborate earlier measurements of pH_{ves} in PMCs, showing the majority of endocytotic vesicles with alkaline pH³². Vesicular pH recordings during changes in pH_e revealed a permeability for protons between the lumen of the vesicles and the extracellular space. For example, a drop in pH_e from 8 to 6 led to an average decrease in pH_{ves} by 1 pH unit, attesting to a significant permeability of this intracellular compartment to protons. Permeabilization of all membranes by the H^+/K^+ ionophore Nigericin and depolarization of the negative V_{M} further enhanced H^+ permeability between the vesicles and the environment, indicating that pH_{ves} is at least partly shielded by the surrounding membranes. In contrast, pH_i is less shielded against changes in environmental pH, revealing a drop by ~ 2 pH units when seawater pH changes from 8 to 6. This high H^+ permeability of the plasma membrane can be attributed to the presence of the H^+ channel Otop2l, which has been previously identified as an exit route for H^+ liberated by the mineralization process in PMCs⁸. However, while the plasma membrane of PMCs is highly permeable to H^+ , the vesicular compartments seem to be partly shielded against changes in pH_e .

A similar H^+ permeability of the plasma membrane has been demonstrated for the calcifying coccolithophores *E. huxleyi* and *Coccolithus pelagicus*, which is largely attributed to the presence of the voltage-gated H^+ channel Hv1^{27,31}. Although a Hv1 homolog is also found in the genome of *S. purpuratus*, our single-cell transcriptomic analyses demonstrate almost no expression of this gene, while Otop2l is expressed highly and exclusively in the PMCs of the sea urchin larva. Interestingly, the permeability of this putative Hv1 channel in coccolithophores is reduced under acidified conditions resembling near-future OA, suggesting a protective mechanism in place to reduce inwardly directed H^+ flux into the cell⁹. Similar to the situation in coccolithophores, acidified conditions simulating CO_2 -driven OA also elicited a down-regulation of Otop2l at the mRNA level in the sea urchin larva⁸. In the same study, the sea urchin Otop2l was demonstrated to exhibit strong pH gating, with acidic conditions inhibiting the channel activity, suggesting a similar protective mechanism as described for coccolithophores. We propose that the calcifying cells of the sea urchin larva have significant H^+ permeability that also governs the pH of endocytotic vesicles. This H^+ permeability through selective channels can allow exit of H^+ generated during the mineralization process from the intracellular site of mineralization (i.e., vesicle) to the surrounding seawater along an electrochemical gradient determined by H^+ concentration differences across the vesicular and plasma membranes. In addition, proton fluxes can be further modulated by the V_{M} , allowing the cell to offset such H^+ gradients across membranes.

Given the relatively stable pH conditions in marine systems over long evolutionary timescales¹, we propose that sea urchin larvae evolved an “open” system for the intracellular formation of CaCO_3 . At a seawater pH of 8.1, the employment of H^+ channels can be regarded energetically advantageous in contrast to ion pumps and secondary active transporters to keep outward-directed H^+ gradients, and thus may represent a positive selection factor during the evolution of mineralizing systems in marine habitats.

H^+ transport in the calcifying cells is modulated by the plasma V_{M}

The V_{M} is a fundamental requisite for the function of all cells³³. V_{M} s are generated by ion channels, electrogenic antiporters, and ion pumps. While ion pumps like the Na^+/K^+ -ATPase and the V-type H^+ -ATPase can generate electrochemical gradients by moving ions across membranes in an energy-requiring mode, channels and antiporters contribute to the V_{M} by a semi-permeable conductance of specific ions down their respective concentration gradient. In most cells, the bulk of the negative plasma V_{M} is maintained by the presence of K^+ channels, allowing K^+ efflux and establishment of an electrochemical equilibrium that follows the Nernst equation. This equation denotes that for a ten-fold difference in monovalent ion (e.g., K^+ , Na^+ , Cl^- , and H^+) concentration across the plasma membrane, selective permeability for one of these ions will generate a V_{M} of -61 mV. In reverse, a V_{M} can also help generate ion concentration differences (i.e., driving force for H^+ gradients) across the plasma membrane in the presence of a H^+ conductance pathway.

In the current study, recordings of PMC plasma V_{M} during changes in extracellular Cl^- , Na^+ , and K^+ demonstrated an appreciable depolarization of the cell during elevation of external K^+ . This indicates that K^+ gradients across the plasma membrane contribute substantially to the establishment of a negative V_{M} in PMCs. Calculations of the V_{app} revealed a V_{app} of -26 mV, which is in good accordance with previously reported V_{M} of -20.6 mV in PMCs using electrode measurements⁸. The magnitude of depolarization of PMCs by high external $[\text{K}^+]$ was reduced in the presence of Ba^{2+} , a broad K^+ channel blocker, suggesting a contribution of K^+ channels to the overall V_{M} .

To test the dependence of pH_i regulation on the plasma V_{M} , we depolarized PMCs in combination with pH_i recordings. Depolarization of the PMC plasma membrane led to an increase in pH_i by 0.5 pH units, indicating a direct interaction between V_{M} and pH_i . In fact, theoretical calculation using the Nernst equation of expected pH changes during full depolarization of V_{M} (i.e., -25 mV) would lead to an increase in pH_i by 0.41 pH units. Based on the good match between our direct pH measurements and theoretical calculations, we conclude that pH_i is strongly dependent on the plasma V_{M} , underlining the role of voltage-independent proton channels (e.g., Otop2l) in mediating proton conductance across the PMC plasma membrane. Patch-clamp experiments in *C. pelagicus* also demonstrated proton currents that were modulated by voltage ramps across the plasma membrane following the Nernst potential for H^+ ²⁷. These findings demonstrate that the V_{M} in

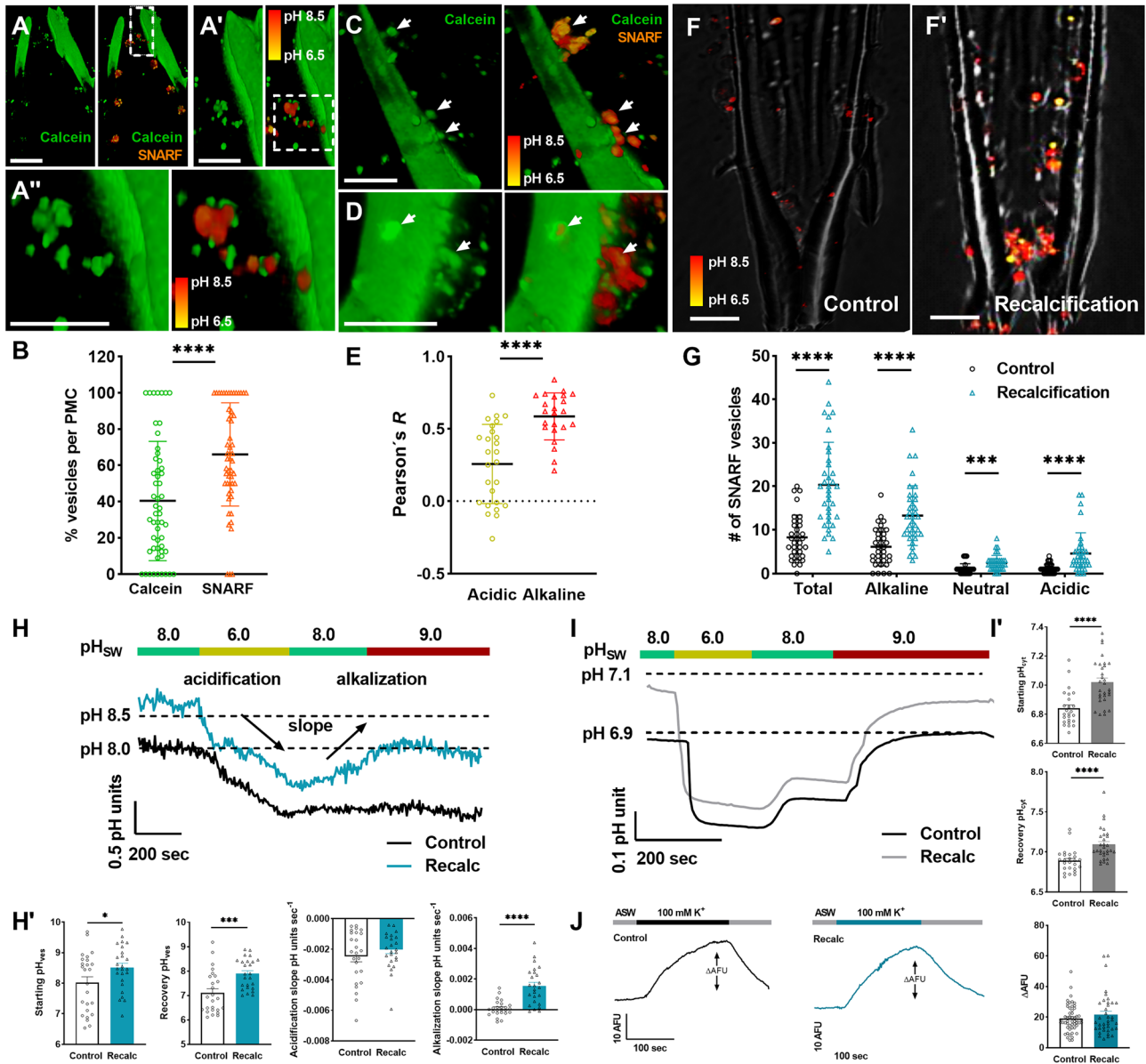


Fig. 4 | Co-localization of endocytotic calcium vesicles with pH_{ves} in the calcifying primary mesenchyme cells (PMCs) of the sea urchin larva. Simultaneous labeling of calcium (calcein) and pH (carboxy-SNARF) in the vesicles of the PMC bodies and syncytial cords. Scale bar: 25 μm (A) and 10 μm (A', A''). **B** Percentage of calcein and SNARF-positive vesicles within the total number of either dye-containing vesicles. Values presented for individual cells as mean \pm SEM ($N = 54$), **** $P < 0.0001$, unpaired t -test. **C** An example of calcium-rich spicule and vesicles that are partially co-localized with SNARF in the PMC body and syncytial extensions (arrows). Scale bar: 10 μm . **D** High magnification image of one PMC with predominantly alkaline vesicles and their co-localization with calcium-rich vesicles (arrows). Scale bar: 10 μm . **E** Pearson's R co-localization analysis of calcein-positive vesicles with alkaline and acidic vesicles, where +1, 0, and -1 indicates 100%, 50%, and 0% co-localization, respectively. Values presented for individual cells as mean \pm SEM ($N = 26$ acidic; $N = 23$ alkaline), **** $P < 0.0001$, unpaired t -test. **F, F'**

Representative images of SNARF-positive vesicles along the spicules of 5 dpf-old control and re-calcifying larvae. Scale bar: 25 μm . **G** Abundance of SNARF-containing vesicles in control and re-calcifying PMCs. Values presented for individual cells as mean \pm SEM ($N = 34$ control; $N = 36$ re-calcification), **** $P = 0.0002$, **** $P < 0.0001$, unpaired t -test. **H, H'** Representative traces and measurements of pH_{ves} changes in response to changes in pH_e in control and re-calcifying PMCs. Values presented for individual cells as mean \pm SEM ($N = 25$ control; **** $P = 0.0469$, **** $P = 0.0006$, **** $P < 0.0001$, unpaired t -test. **I, I'** Representative traces and measurements of pH_i changes in response to changes in pH_e in control and re-calcifying PMCs. Values presented for individual cells as mean \pm SEM ($N = 25$ control; $N = 30$ re-calcification), **** $P < 0.0001$, unpaired t -test. **J** Representative traces and measurements of changes in PMC plasma membrane depolarization intensity in control and re-calcifying larvae. Values presented for individual cells as mean \pm SEM ($N = 53$ control; $N = 38$ re-calcification), unpaired t -test.

the calcifying cells of sea urchin larvae and coccolitophores represents a master modulator of proton transport across the plasma membrane. At a normal seawater pH of 8.2, PMCs with a pH_i of 7.0 and a V_M of -20 mV maintained by K^+ channels exhibit a net outward H^+ motive force across the plasma membrane. In theory, this outwardly directed H^+ transport would reverse when pH_e drops below 7.6. Thus, to protect themselves from acidosis during reduced seawater pH, the cells could

respond by shifting to a more positive V_M or by decreasing H^+ conductivity via H^+ channels. The latter is supported by our observation that Otop2l had reduced expression levels when larvae were raised under acidified (pH 7.4) conditions compared to control animals raised at pH 8.1⁸. Another line of evidence for pH gating of H^+ permeability in the PMCs comes from heterologous expression experiments where H^+ currents conducted by Otop2l in oocytes demonstrated Otop2l

inactivation under near-neutral and acidic conditions⁸. Interestingly, here we show that increases in pH_i by depolarization of the cell did not elicit any detectable pH changes on the vesicular level. We assume that these minor increases in pH_{ves} remained undetectable due to the lower resolution of the pH-sensitive dye under highly alkaline vesicular conditions. Taken together, our results demonstrate that the plasma V_M is a key regulator of pH_i in PMCs. Employment of the V_M in concert with H^+ channels represents a highly energy-efficient mechanism to maintain pH_i homeostasis, which, however, requires stable pH_e conditions.

High pH, Ca^{2+} , and Mg^{2+} activate Otop2l proton channels that is responsible for H^+ permeability in PMCs

The sea urchin Otop2l has been identified as an H^+ selective ion channel in the PMCs, where it is activated by alkaline conditions⁸. In the present work, we performed an in-depth analysis of Otop2l activation by pH and divalent cations. Heterologous expression of Otop2l in oocytes demonstrated an activation of the channel by alkaline conditions $>pH 7.4$ and an attenuation of this activation when exceeding pH 9.2. This demonstrates that alkaline conditions far beyond natural seawater pH (i.e., pH 7.9–8.3) stimulate the activity of this channel. The murine otopetrins, including Otop1 and Otop2, were demonstrated to be steeply activated by extracellular H^+ , corroborating the central role of Otop1 in the sour taste receptors^{28,34}. However, murine Otop2 is active over a wide pH range from 5 to 10 and is characterized by outward currents in response to extracellular alkalization ($>pH 9$)³⁵. This indicates evolutionarily conserved features of the sea urchin and murine Otop2 in promoting the export of protons across the plasma membrane.

Our results show that high external Ca^{2+} and Mg^{2+} can additionally stimulate H^+ conductivity of this channel. Strikingly, even under low pH conditions of 7.4, when Otop2l exhibits no detectable H^+ currents, addition of Mg^{2+} to the external bath solution substantially activated this H^+ channel, as did natural seawater Ca^{2+} concentrations under pH 8.5. Our immunolabeling analysis confirmed the presence of Otop2l not only in the PMC plasma membrane but also within large interconnected vacuoles that are predominantly found in the cell bodies of actively calcifying regions like the sheitel and the rod tips. This vesicular network has striking similarities with the one observed by cryo-EM analysis, which has been proposed to be involved in the endocytotic calcium uptake into PMCs and subsequent ACC formation^{22,36}. We also detected smaller Otop2l-positive vesicles throughout the syncytial cables running along the skeleton, where calcification takes place. Based on these observations, we conclude that the proton channel Otop2l, which has been demonstrated to mediate H^+ efflux from the cytoplasm⁸ is also localized in membranes of large subcellular vacuoles and vesicles. We propose that during seawater endocytosis, Otop2l localized in the plasma membrane is incorporated into the membranes of these vesicles and vacuoles in which ACC is formed⁹. Given the necessity to concentrate calcification substrates, including Ca^{2+} , Mg^{2+} , and CO_3^{2-} in these calcification vesicles¹⁹ it is tempting to speculate that Otop2l activity is stimulated under these conditions, thus increasing vesicular H^+ permeability. This hypothesis is supported by our heterologous Otop2l characterizations that demonstrated activation of the H^+ channel by alkaline pH and Ca^{2+} concentrations far beyond seawater conditions (i.e., pH 9.5, 100 mM Ca^{2+}). This modulation of H^+ permeability in vesicular membranes could be beneficial to maintain high pH in the calcification vesicle and thereby promote carbon concentration and $CaCO_3$ formation. The latter hypothesis is supported by our Otop2l knock-down experiments, revealing attenuated changes in pH_{ves} during changes in pH_e in Otop2l morphants compared to control animals. At this point, we cannot specifically attribute the changes in proton permeability across the vesicular membrane to the function of Otop2l, since the reduction in proton permeability in Otop2l morphants may be solely due to decreased H^+

flux across the plasma membrane. Our data point to a role of Otop2l in modulating membrane H^+ permeability in the PMCs with potential function in regulating pH_{ves} during ACC formation.

H^+ permeability and abundance of alkaline, calcium-rich vesicles are increased during calcification

Calcein has been widely used to track the route of calcium uptake into the calcifying cells of the sea urchin larva and other calcifying organisms^{20,22,37}. Cell surface labeling experiments support calcein uptake by endocytosis into the large vesicles within PMCs³⁸, and correlative microscopy techniques have shown that calcein-labeled vesicles inside PMCs and their filopodial cables contain ACC²². Our calcein labeling experiments performed on early pluteus larvae confirmed a rapid uptake of the dye and incorporation into the skeleton within 2–3 h. Simultaneous measurements of pH_{ves} using carboxy-SNARF demonstrated that calcein-rich vesicles partially co-localize with the pH dye, suggesting that the uptake and processing of vesicles follow similar endocytosis mechanisms. However, we cannot neglect the relatively high number of vesicles that showed no co-localization of the two dyes (i.e., Fig. 4B, Figs. S11–S13). We explain this finding by: (i) a post-endocytotic sorting of the dyes, or (ii) a slight temporal delay in endocytotic uptake of the dyes due to their different molecular mass (i.e. calcein: 994.86 g M^{-1} and carboxy-SNARF: 568 g M^{-1}) causing different speed of diffusion across the ectoderm and the proteoglycan matrix of the primary body cavity, or (iii) a depletion of Ca^{2+} ions from SNARF-positive vesicles. Interestingly, we often observed large vacuolar-like structures containing both dyes and surrounded by a number of smaller vesicles that only had calcein (Figs. S11, S12, Movies S1–S4). These large vacuoles were alkaline and mostly found within the PM cell bodies. Our observations corroborate earlier findings reporting an extensive network of connected endocytotic vesicles and vacuoles close to the surface of PMCs that endocytose seawater-like fluids from the extracellular matrix^{22,36}. Within the syncytial cables, we observed smaller vesicles, and co-localization analyses indicate a higher association of Ca^{2+} -rich vesicles with alkaline vesicles than with those characterized by near-neutral or acidic pH conditions. In our time-lapse recordings, we saw alkaline, calcein-positive vesicles within the syncytial cables that fused with the luminal membrane facing the skeleton, which resembles the proposed exocytosis of ACC vesicles (Movies S1–S4). We also observed incorporation of SNARF into the skeleton, as it has been reported for other fluorescent dyes used to track endocytosis in PMCs³⁸. Interestingly, SNARF dye deposited in the skeleton revealed alkaline pH ($>pH 8$) within the freshly formed mineral surrounded by the PMC syncytial cables. The latter observation provides an insight into the pH conditions at the mineralization front in the sea urchin larva and thereby supports a combined calcification mode including ion-by-ion growth and particle attachment. Similar alkaline conditions were described for corals, and mussel larvae within the calcifying fluids at the tissue mineral interface^{12,13}, and recent observations also point towards a combination of vesicular ACC precursor formation in concert with an elevation of the carbonate saturation state in the privileged space at the skeleton-tissue interface².

We further discovered that skeleton regeneration, which reflects a highly active PMC calcification state, is associated with increased abundance of endocytotic vesicles compared to non-re-calcifying PMCs. While the majority of the vesicles were alkaline, the number of neutral and acidic vesicles also increased significantly in re-calcifying PMCs. These different vesicle populations may reflect vesicles with high Ca^{2+} and CO_3^{2-} saturation state as well as vesicles with low pH, which may transport acidic matrix proteins^{39,40}. Strikingly, the average pH of vesicles was markedly increased in re-calcifying PMCs, which was accompanied by their increased permeability to H^+ . Analogous to the situation in vesicles, the pH_i was also elevated in re-calcifying PMCs, which is in accordance with previous observations of increased pH_i in

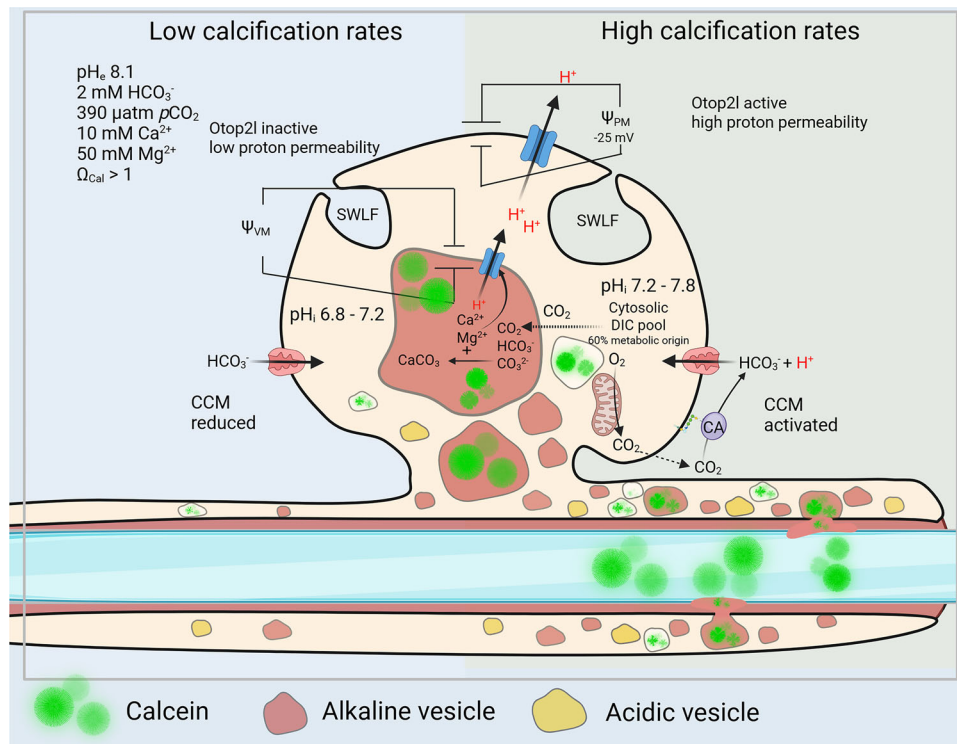


Fig. 5 | A working model for the intracellular calcification mechanism in the sea urchin larva. Calcifying PMCs exhibit a pronounced H⁺ permeability of the plasma membrane due to the presence of Otop21 H⁺ channel that is activated by Mg²⁺, Ca²⁺, and alkaline pH. The V_M is a strong modulator of pH_i, which increases during calcification. In contrast to PMCs that have a low calcification rate (e.g., PMCs of older larvae), PMCs of early pluteus larvae or re-calcifying larvae have high H⁺ permeability and elevated pH_i and pH_{ves}. Stimulation of calcification is accompanied by a higher abundance of alkaline and acidic endocytotic vesicles partially co-localizing with Ca²⁺ dye calcein. Carbon concentration in PMCs by extracellular

carbonic anhydrase in concert with Na⁺/HCO₃⁻ cotransporter^{24,25} helps increase the cellular carbon pool in calcifying PMCs. A more alkaline pH_{ves} compared to the cytoplasm provides a positive CO₂ gradient from the cytosol into these vesicles, thereby trapping CO₂ as HCO₃⁻ and CO₃²⁻. Calcein and SNARF fluorescence in the calcitic spicule, together with the observation of vesicles in the direct vicinity of the cell-spicule interface, provide evidence for the process of exocytosis towards the skeleton. Incorporation of SNARF into the skeleton reflects high pH conditions at the site of mineral formation within the syncytial cables. Created in BioRender. <https://BioRender.com/1ecnppp>.

actively calcifying PMCs^{25,32}. Our V_M measurements did not detect any differences between control and re-calcifying PMCs, suggesting that the elevation in pH_i is likely due to an enhanced bicarbonate uptake to increase the cellular carbon pool, as suggested previously^{25,32}. Even under elevated pH_i, the outwardly directed H⁺ gradient and a membrane potential of -25 mV would still promote efflux of H⁺ from the cell. However, at a pH_i of 6.8–7.3, vesicular alkalinization up to pH 8.5 would only be possible by a lumen-positive V_M driving H⁺ out of the vesicle against a concentration gradient. Given a similar ion composition in the calcification vesicle membrane as in the plasma membrane and similar ionic gradients, the vesicle membrane would have a lumen-positive potential of 25 mV. This would explain the alkalinization of the vesicle by 0.42 pH units higher than the pH_i. Using Di-8-Anepps, a V_M probe that emits fluorescence when integrated into the outer leaflet of the plasma membrane, we observed strong fluorescence in calcein-positive endocytotic vesicles. Due to the membrane-impermeant nature of the dye, internalization can only happen by endocytosis, and the strong fluorescence of this dye in the vesicles compared to the plasma membrane points towards a high lumen-positive potential that may enable further alkalinization of the vesicles. However, quantitative measurements of vesicular membrane potential are needed to precisely explain the electrochemical driving forces for luminal alkalinization in endocytotic vesicles. Given relatively high vesicular H⁺ conductivity, an elevation in pH_i can improve outward-directed H⁺ gradients from vesicles and thereby support CO₃²⁻ formation. These findings are summarized in Fig. 5, illustrating the interaction of cellular H⁺ permeability, V_M, and seawater endocytosis in different calcification states.

Our calcein and carboxy-SNARF pulse-chase experiments strongly underline a major role of seawater vacuolization in the calcification process of the sea urchin larva. Some of the endocytosed vesicles maintain a high pH that would support an increase in the carbonate saturation state within these subcellular compartments. The effect of carbon concentration in these vesicles is further enhanced by lower pH_i and high CO₂ partial pressure, leading to an influx and trapping of CO₂ in these alkaline compartments. A similar model for CO₂ trapping in alkaline vacuoles has been proposed for hyaline and miliolid foraminifera that were also demonstrated to utilize metabolic CO₂ as a major carbon source to build their calcareous shells^{41–43}. Tracking of carboxy-SNARF and calcein provides compelling evidence that vesicles containing alkaline conditions and calcium ions are exocytosed into the lumen of the syncytial cables, where the calcitic skeleton is formed.

A deep evolutionary origin of intracellular calcification suggests the existence of conserved mechanisms of mineralization processes³. The identification of the unifying mechanisms underlying calcification has been a top research priority in the context of climate change to make large-scale predictions and explanations for sensitivities of marine calcifiers to changes in seawater carbonate chemistry in the past and future oceans¹⁰. However, such large-scale predictions are impossible without understanding the mechanisms underlying the intracellular formation of CaCO₃. Here we demonstrated that calcifying cells of the sea urchin larva possess a high H⁺ permeability that directly affects pH conditions in endocytotic, calcium-rich vesicles, which are likely the site of mineral precursor formation. This high H⁺ permeability allows H⁺ generated by the vesicular formation of ACC to exit the calcification vesicle and the cytoplasm along electrochemical

gradients. This mechanism is energetically inexpensive since it relies on fundamental cellular features, including the V_M and natural H^+ gradients. However, stable pH conditions in oceanic environments over long evolutionary timescales are a critical factor to employ such an “open” H^+ channel-based calcification mechanism. Thus, rapid changes in oceanic pH as described during mass extinction events in the Earth’s history or future OA conditions may pose a significant challenge to these calcifying systems.

Methods

Ethical statement

The use of *X. laevis* was licensed by the authorities (Ministerium für Landwirtschaft, ländliche Räume, Europa und Verbraucherschutz, Tierversuchsanzeige IX 555 – 106759/2023 (33-6/23V), Schleswig-Holstein, Germany). No ethical approval was required for work with sea urchins and their larval stages. This work complies with European and institutional ethical standards and does not require formal ethical approval beyond standard institutional oversight for marine invertebrate research.

Experimental animals and larval cultures, and their calcification assay

Adult purple sea urchins (*Strongylocentrotus purpuratus*) were collected from the coast of California (La Jolla, CA) and shipped to the Helmholtz Centre for Ocean Research Kiel (GEOMAR). The animals were maintained in a recirculating natural seawater system at 12 °C, a salinity of 32, and regular water changes were made three times a week. Animals were fed with *Laminaria* sp. three times a week. Spawning of males and females was induced by gentle shaking, eggs were fertilized, and larval cultures were maintained at a concentration of 25,000 larvae/L at 15 °C with continuous aeration. For all experiments, 3–4 dpf (days post-fertilization) old larvae of unknown sex were used since they are too small to differentiate at this stage. The re-calcification assay was performed by exposing 3dpf larvae to 2-(N-morpholino)ethanesulfonic acid (MES)-buffered (30 mM) filtered sea water (FSW) adjusted to pH 6 to dissolve their skeletons. After 9 h, larvae were transferred back to fresh FSW (pH 8.1) to regenerate their calcitic endoskeleton.

Intracellular pH (pH_i) and vesicular pH (pH_{ves}) recordings

Intracellular pH recordings and calibrations were performed using the ratiometric pH-sensitive dye BCECF-AM. For cytosolic as well as intravesicular pH measurements, the ectoderm of the larvae was removed using a bag-isolation protocol⁴⁴. Therefore, larvae were exposed to three washes of dissociation medium (1 M glycine, 100 μM EDTA, pH 8.0) followed by two washes in bag-isolation medium (40% Ca²⁺/Mg²⁺-free artificial sea water (ASW), 40% 1 M dextrose, 20% distilled water, pH 8.0). For dye loading, larvae were incubated in FSW containing 10 μM of BCECF-AM dissolved in DMSO^{21,24,25}. pH measurements within endocytotic vesicles were conducted using the membrane-impermeable BCECF-10kDa dextran or carboxy-SNARF that can be used for ratiometric measurements of pH in aqueous solutions. For both dyes, a 250 mM stock solution was prepared using DMSO as a solvent and applied to the larvae at a final concentration of 250 μM. Larvae were incubated in the staining solution for 1–2 h to take up the membrane-impermeable dyes by endocytosis. Larvae were transferred to a protamine-sulfate-coated coverslip that was glued onto a perfusion chamber using silicon grease. For vesicular pH measurements, the perfusion chamber was mounted to the stage of a Leica Stellaris inverted confocal microscope equipped with a temperature-controlled perfusion system. SNARF recordings were conducted by setting the excitation laser to 550 nm and dual emission filters at 580 nm and 645 nm for ratiometric measurements. For BCECF recordings, the fluorescence was monitored using an inverted Zeiss microscope (Observer A1) equipped with VisiTron imaging software

and 455 nm and 505 nm dual excitation and 520 nm emission wavelengths.

Intracellular and vesicular PMC proton permeability experiments were performed by perfusing the cells with filtered seawater (FSW) containing different pH (pH 6, 7, 8, 9). pH of FSW was buffered by the addition of 30 mM 2-(N-Morpholino)ethanesulfonic acid (MES) or 10 mM Tris(hydroxymethyl)aminomethane (TRIS) and adjusted by the addition of HCL or NaOH. For translation of dye fluorescence ratios into actual pH values, a Nigericin calibration was performed where cells were exposed to ASW solutions adjusted to different pH conditions (5.0; 6.0; 7.0; 8.0; 9.0; 9.5) in the presence of 10 μM nigericin and high external [K⁺] (100 mM) (Table S2)^{21,24,32}.

V_M measurements

The V_M of PMCs was measured using the anionic potential-sensitive dye DiBAC₄³ (Bis-(1,3-Dibutylbarbituric Acid)Trimethine Oxonol; AAT Bioquest). A 50 mM DiBAC stock was prepared in distilled water and used at a final concentration of 100 nM. For the measurements, larval ectoderm was removed as described earlier using the bag-isolation method, and the PMCs were pre-incubated in seawater with DiBAC for 0.5 h. To depolarize the PMC membrane, an artificial seawater (ASW; Table S1) containing 30 mM, 60 mM, and 100 mM K⁺ was tested, and a final 100 mM K⁺ ASW (Table S2) was used for subsequent experiments. ASW solutions with modified Na⁺ and Cl⁻ concentrations (Tables S3 and S4) were also tested but had no effect on PMC V_M (Fig. 2E). To further examine the effect of K⁺ conductance on PMC V_M , 1 mM of K⁺ channel blocker Ba²⁺ was used. During perfusion measurements, all solutions contained 100 nM of DiBAC. DiBAC fluorescence was monitored using a Leica Stellaris inverted confocal microscope equipped with LAS-X life-cell imaging software, and with a 488 nm excitation laser and 535-565 bandpass emission filter.

Based on the fluorescence intensities of the membrane-permeable anionic DiBAC₄³ dye under resting conditions and depolarization by high [K⁺], we estimated the V_{app} according to the modified Nernst equation as previously described for anionic V_M dyes⁴⁵:

$$E_{Nernst} = \frac{RT}{zF} \ln \frac{Dye\ fluorescence\ resting}{Dye\ fluorescence\ depolarization}$$

With R: ideal gas constant, T: temperature in Kelvin, F: Faraday constant, and z: charge of the ion.

Since DiBAC₄³ is fluorescent only in the cytoplasm, calculation of V_{app} is based on the condition that during depolarization [DiBAC₄³]_i is the same as [DiBAC₄³]_e and thus reflects the extracellular concentration of the dye. In addition, di-8-ANEPPS was used to estimate the V_M of endocytotic vesicles. Di-8-ANEPPS emits fluorescence when incorporated into the outer leaflet of the plasma membrane, and endocytosis leads to the appearance of the dye in the vesicles. Di-8-ANEPPS was dissolved in DMSO to obtain a 10 mM stock solution. After removal of larval ectoderm as described earlier, larvae were incubated at a final concentration of 10 μM for 30 min. For double staining, larvae were incubated in 10 μM di-8-ANEPPS and 250 μM calcein for 1 h. Afterward, larvae were washed three times with filtered seawater (FSW) and imaged on a Leica Stellaris confocal microscope using the appropriate excitation (468 nm) and emission (633 nm) wavelengths.

Life-cell imaging using calcein and pH dyes

Pulse-chase experiments using membrane-impermeable carboxy-SNARF and calcein were performed by incubating larvae for 2–3 h in filtered seawater (FSW) containing 125 μM carboxy-SNARF or/and 250 μM calcein. After incubation, larvae were immobilized by the bag-isolation method as described above and mounted onto a protamine-coated coverslip in a perfusion chamber containing FSW. Larvae were imaged on a Leica Stellaris inverted confocal microscope equipped with a 3D image visualization and analysis module. After 3D

reconstruction, images were analyzed by ImageJ using the co-localization plugin to analyze the degree of co-localization of calcein and SNARF-containing vesicles. For co-localization analyses, single cells were cropped into rectangles to reduce the surrounding background area. Pearson's correlation coefficient above threshold was calculated using ImageJ and dissection threshold regression. Pearson's R was plotted for single cells (each dot represents one cell) from five larvae.

Immunohistochemistry

Immunofluorescence analysis was performed using a polyclonal primary antibody generated against a synthetic peptide corresponding to the C-terminal region (CLDAMHRKPPEDFKQTR) of sea urchin Otop2l⁸. Briefly, larvae were fixed in 4% paraformaldehyde in FSW, blocked using 5% bovine serum albumin in PBST (PBS with 0.3% Tween20), and incubated overnight at 4 °C with primary antibody diluted 1:250. After washing in PBST, samples were incubated with Alexa Fluor 488 conjugated anti-rabbit IgG (Invitrogen) secondary antibody for 1 h at a 1:400 dilution, and pictures were taken on a confocal microscope equipped with Airyscan function (LSM800/P2, Zeiss, Germany).

Morpholino knock-down

Morpholino knock-down of Otop2l was performed and validated in a previous study⁸. Knock-down was performed using the gene-specific morpholino-substituted antisense oligonucleotides (MO) 5'-GTTGTTGCCGAAATTATACGCTTAG-3' complementary to the 5' UTR sequence ahead of the sea urchin Otop2l (LOC579173) start codon, including a negative control by using a scramble MO that has no biological target in the sea urchin. MOs were obtained from Gene Tools (Oregon, USA). The MO was dissolved in 0.5 M KCl solution and was injected into the fertilized egg (1 cell stage) using a microinjection system (Picospritzer III, Parker, USA) mounted on an inverse microscope (Zeiss ObserverD1) equipped with a cooling stage⁴⁶.

Heterologous characterization of Otop2l in oocytes and HEK293 cells

Oocyte lobes were surgically removed from female *Xenopus laevis* frogs anesthetized with tricaine. Connective tissue was digested with 2 mg/ml collagenase type II (Merck) in (in mM): 82.5 NaCl, 2 KCl, 1 MgCl₂, 5 HEPES (pH 7.5) for 1 h at room temperature. Isolated oocytes were washed and stored at 17 °C in OR2 solution (in mM): 96 NaCl, 2 KCl, 1.8 CaCl₂, 1 MgCl₂, 5 HEPES (pH 7.5)⁴⁷. The husbandry conditions, surgical protocol, aftertreatment procedures, as well as abortion/euthanasia criteria, are supervised by the animal welfare officer of Kiel University.

The coding sequence for Otop2l (Genbank accession SPU_004766) was subcloned into the dual-purpose vector pFAW, which contains a T7 promoter as well as 5' and 3' UTRs as enhancer sequences for oocyte expression and a CMV promoter for expression in cultured cells. For oocyte expression, the plasmid was linearized with MluI, and capped cRNA was transcribed in-vitro using the T7 AmpliCap Max High Yield Message Maker Kit (Cellscript). cRNA integrity was verified by gel electrophoresis, its concentration was determined photometrically, and stock solutions were stored at -80 °C. Oocytes were injected with ~50 nl of cRNA for Otop2l (100 ng/μl) and incubated for 7 to 8 d at 17 °C in (in mM): 54 NaCl, 30 KCl, 2.4 NaHCO₃, 0.82 MgSO₄, 0.41 CaCl₂, 0.33 Ca(NO₃)₂, 7.5 Tris (pH 7.5) supplemented with 100 U/ml Penicillin and 100 μg/ml Streptomycin. For expression in mammalian cells, HEK293 cells were obtained from ATCC and cultured at 37 °C/5% CO₂ in Dulbecco's modified Eagle medium (DMEM) supplemented with 10% fetal calf serum (FCS) and Penicillin/ Streptomycin. Cells with 70% confluency were transiently transfected with 1 μg Otop2l and 0.1 μg EYFP constructs per well (24-well plate) using Lipofectamine 2000 (Invitrogen) or FuGENE (Promega) according to the manufacturer's instructions. Cells were incubated for 18–24 h, dissociated with trypsin/EDTA, and seeded onto

sterile 10 mm glass coverslips 2–6 h prior to electrophysiological recordings.

Two-electrode voltage-clamp (TEVC) recordings

All recordings were performed at room temperature with a HEKA multielectrode clamp amplifier iTEV90 (HEKA Electronics) or a TURBO TEC 10CX amplifier (NPI Electronic Instruments). Data were sampled at 10 kHz and filtered with 3 kHz (-3 dB)⁸. Microelectrodes were pulled from borosilicate glass capillaries (GB200F-8P, Science Products), filled with 3 M KCl, and had a resistance of 0.5–1.2 MΩ. For current measurements, the V_M was held at -80 mV, and voltage ramps from -100 mV to +60 mV (1 s duration) were applied with a sweep interval of 2 s. Data were acquired with PatchMaster (HEKA Electronics) and analyzed with FitMaster (HEKA Electronics), IgorPro 8 (WaveMetrics), and Prism (GraphPad Software). Recording solutions for pH activation experiments contained (in mM): 120 KCl, 1.8 CaCl₂, 2.0 MgCl₂, and 10 HEPES (pH 7.4–7.8), 10 Ampso (pH 8.2–9.8), or 10 MES (pH 4.0–6.0), respectively. Recording solutions for Mg²⁺ activation experiments contained (in mM): 120 KCl, 10 HEPES, and 1–50 MgCl₂ as indicated in the experiment descriptions (pH 7.4).

H⁺-selective microelectrodes were used to monitor pH_i in oocytes during changes in pH_e. Borosilicate glass micropipettes with tip diameters of 2–3 μm were vapor-silanized with dimethyl chlorosilane (Sigma-Aldrich) and front-loaded with a 200-μm column of liquid ion exchanger mixture (H⁺ ionophore III; Sigma-Aldrich) diluted in 2-nitrophenyl ether at a concentration of 10.5 mg·mL⁻¹. Micropipettes were additionally front-loaded with a 50-μm column of the ionophore mixture containing a polyvinylchloride/tetrahydrofuran (330 mg mL⁻¹) solution with a ratio of 1:3 to seal the opening of the electrode tip. The micropipette was backfilled with electrolyte solution (300 mM KCl, 50 mM NaPO₄, pH 7). To calibrate the ion-selective probe, each microelectrode was calibrated by measuring the Nernstian property of each microelectrode in a series of pH solutions (pH 6, 7, 8, and 9) with reference to an Ag/AgCl electrode. For all electrodes, a Nernstian slope of >51 mV for 1 pH unit was obtained^{21,48}. For pH_i measurements, oocytes were placed in a perfusion chamber on a temperature-controlled (17 °C) inverted microscope. The microelectrode was gently inserted into the vegetative pole of the oocyte, and pH_i was recorded during changes in pH_e at a similar rate and duration as in the TEVC measurements.

Patch-clamp recordings of HEK293 cells

All recordings were performed at room temperature in the whole-cell configuration, and extracellular solutions were exchanged using a multi-barrel application system. Pipettes were pulled from thin-walled borosilicate glass (GB150TF-8P, Science Products) and had resistances of 1.2–1.9 MΩ when immersed in standard extracellular solution. Currents were recorded with an EPC10 amplifier controlled by PatchMaster (both HEKA Electronics) at a sampling rate of 10 kHz and filtered with 2.9 kHz. Cells were held at -80 mV, and currents were elicited by a voltage ramp (duration 200 ms) from -100 to +100 mV every 5 s. Currents were analyzed with PatchMaster (HEKA Electronics), IgorPro 8 (Wavemetrics), and Prism (GraphPad Software).

Standard extracellular solution contained (in mM): 145 NaCl, 5 KCl, 1 MgCl₂, 2 CaCl₂, 10 dextrose, 10 HEPES (pH 7.4) or 10 AMPSO (pH 8.5), respectively. For Ca²⁺ activation experiments, the extracellular solution contained (in mM): 145 NaCl, 5 KCl, 1 MgCl₂, 10 dextrose, 0–100 CaCl₂ as indicated in the experiment descriptions, and 10 HEPES (pH 7.4) or 10 AMPSO (pH 8.5). The intracellular solution contained (in mM): 140 CsCl, 2 MgCl₂, 1 CaCl₂, 2.5 EGTA, 10 HEPES (pH 7.3). Cs⁺ was chosen in order to suppress background currents in HEK293 cells.

Statistical analyses

All data were checked for normal distribution and analyzed for significance using GraphPad Prism 8. Effects of pH_e on Nigericin

treatment, cytosolic and pH_{ves} , acidic and alkaline vesicles, Otop21 knock-down, as well as V_M and re-calcification measurements were tested using unpaired two-sided Student's *t*-test with $P \leq 0.05$. All experiments and measurements were replicated at least three times with individual larval cultures or experimental setups. All figures were generated using GraphPad Prism 8, and statistical analysis results are presented in the figure legends.

Reporting summary

Further information on research design is available in the Nature Portfolio Reporting Summary linked to this article.

Data availability

The data generated in this study are provided in the main text and the Supplementary Information file, and deposited in the DRYAD online data repository [10.5061/dryad.2bvq83bzw]. The scRNA-seq in Supplementary Fig. 2 is taken from a previous publication [Chang et al. 2021 PNAS 118:e2101378118], and the data is deposited in the GEO repository under accession code [GSE322501](https://www.ncbi.nlm.nih.gov/geo/query/acc.cgi?acc=GSE322501).

References

- Zeebe, R. E. History of seawater carbonate chemistry, atmospheric CO_2 and ocean acidification. *Annu. Rev. Earth Planet Sci.* **40**, 141–165 (2012).
- Gilbert, P. U. P. A. et al. Biomineralization: integrating mechanisms and evolutionary history. *Sci. Adv.* **8**, eabl9653 (2022).
- Kahil, K., Weiner, S., Addadi, L. & Gal, A. Ion pathways in biomineralization: perspectives on uptake, transport, and deposition of calcium, carbonate, and phosphate. *J. Am. Chem. Soc.* **143**, 21100–21112 (2021).
- Simkiss, K. & Wilbur, K. M. Biomineralization: cell biology and mineral deposition. *Q. Rev. Biol.* **66**, 75 (1989).
- Furla, P., Galgani, I., Durand, I. & Allemand, D. Sources and mechanisms of inorganic carbon transport for coral calcification and photosynthesis. *J. Exp. Biol.* **203**, 3445–3457 (2000).
- Sikes, C. S., Okazaki, K. & Fink, R. D. Respiratory CO_2 and the supply of inorganic carbon for calcification of sea urchin embryos. *Comp. Biochem. Physiol. A* **70**, 285–291 (1981).
- Bach, L. T., Riebesell, U., Gutowska, M. A., Federwisch, L. & Schulz, K. G. A unifying concept of coccolithophore sensitivity to changing carbonate chemistry embedded in an ecological framework. *Prog. Oceanogr.* **135**, 125–138 (2015).
- Chang, W. W. et al. An otopetrin family proton channel promotes cellular acid efflux critical for biomineralization in a marine calcifier. *Proc. Nat. Acad. Sci. USA* **118**, e2101378118 (2021).
- Kottmeyer, D. M. et al. Reduced H^+ channel activity disrupts pH homeostasis and calcification in coccolithophores at low ocean pH. *Proc. Nat. Acad. Sci. USA* **119**, e2118009119 (2022).
- Pörtner, H. O. et al. *Special IPCC Report on the Ocean and Cryosphere in a Changing Climate* (Cambridge University Press, Cambridge, UK, 2019).
- Jurikova, H. et al. Boron isotope systematics of cultured brachiopods: response to acidification, vital effects and implications for paleo-pH reconstructions. *Geochim. Cosmochim. Acta* **248**, 370–386 (2019).
- Ramesh, K., Hu, M. Y., Thomsen, J., Bleich, M. & Melzner, F. Mussel larvae modify calcifying fluid carbonate chemistry to promote calcification. *Nat. Commun.* **8**, 1709 (2017).
- Sevilgen, D. S. et al. Full in vivo characterization of carbonate chemistry at the site of calcification in corals. *Sci. Adv.* **5**, eaau7447 (2018).
- Mass, T. et al. Amorphous calcium carbonate particles from coral skeletons. *Proc. Nat. Acad. Sci. USA* **114**, E7670–E7678 (2017).
- Sun, C.-Y. et al. From particle attachment to space-filling coral skeletons. *Proc. Nat. Acad. Sci. USA* **117**, 30159–30170 (2020).
- Mount, A. S., Wheeler, A. P., Paradkar, R. P. & Snider, D. Hemocyte-mediated shell mineralization in the Eastern oyster. *Science* **304**, 297–300 (2004).
- Politi, Y., Arad, T., Klein, E., Weiner, S. & Addadi, L. Sea urchin spine calcite forms via a transient amorphous calcium carbonate phase. *Science* **306**, 1161–1164 (2004).
- Beniash, E., Aizenberg, J., Addadi, L. & Weiner, S. Amorphous calcium carbonate transforms into calcite during sea urchin larval spicule growth. *Proc. R. Soc. Lond. B* **264**, 461–465 (1997).
- Kahil, K. et al. Cellular pathways of calcium transport and concentration towards mineral formation in sea urchin larvae. *Proc. Nat. Acad. Sci. USA* **117**, 30957–30965 (2020).
- Vidavsky, N. et al. Initial stages of calcium uptake and mineral deposition in sea urchin embryos. *Proc. Nat. Acad. Sci. USA* **111**, 39–44 (2014).
- Stumpp, M. et al. Acidified seawater impacts sea urchin larvae pH regulatory systems relevant for calcification. *Proc. Nat. Acad. Sci. USA* **109**, 18192–18197 (2012).
- Vidavsky, N. et al. Calcium transport into the cells of the sea urchin larva in relation to spicule formation. *Proc. Nat. Acad. Sci. USA* **113**, 12637–12642 (2016).
- Demertzis, M. A. Fluorimetric determination of calcium in serum with calcein: complexation of calcein with calcium and alkali metals. *Anal. Chim. Acta* **209**, 303–308 (1988).
- Hu, M. Y. et al. A Slc4 family bicarbonate transporter is critical for intracellular pH regulation and biomineralization in sea urchin embryos. *elife* **7**, e36600 (2018).
- Matt, A., Chang, W. J. & Hu, M. Y. Extracellular carbonic anhydrase activity promotes a cellular carbon concentration mechanism in metazoan calcifying cells. *Proc. Natl. Acad. Sci. USA* **119**, e2203904119 (2022).
- Capasso, L., Ganot, P., Planas-Bielsa, V., Tambutté, S. & Zoccola, D. Intracellular pH regulation: characterization and functional investigation of H^+ transporters in Stylophora pistillata. *BMC Mol. Cell Biol.* **22**, 18 (2021).
- Taylor, A. R., Chrachri, A., Wheeler, G. S., Goddard, H. & Brownlee, C. A voltage-gated H^+ channel underlying pH homeostasis in calcifying coccolithophores. *PLoS Biol.* **9**, e1001085 (2011).
- Tu, Y.-H. et al. An evolutionarily conserved gene family encodes proton-selective ion channels. *Science* **359**, 1047–1050 (2018).
- Hughes, I. et al. Otopetrin 1 is required for otolith formation in the zebrafish *Danio rerio*. *Dev. Biol.* **276**, 391–402 (2004).
- Hurle, B. et al. Non-syndromic vestibular disorder with otoconial agenesis in tilted/mergulhador mice caused by mutations in otopetrin1. *Hum. Mol. Genet.* **12**, 777–789 (2003).
- Suffrian, K., Schulz, K. G., Gutowska, M. A., Riebesell, U. & Bleich, M. Cellular pH measurements in *Emiliania huxleyi* reveal pronounced membrane proton permeability. *N. Phytol.* **190**, 595–608 (2011).
- Hu, M. Y., Petersen, I., Chang, W., Blurton, C. & Stumpp, M. Cellular bicarbonate accumulation and vesicular proton transport promote skeleton regeneration in the sea urchin larva. *Proc. R. Soc. Lond. B* **287**, 20201506 (2020).
- Alberts, B., Johnson, A. & Lewis, J. *Molecular Biology of the Cell* 4th edn (Garland Science, New York, 2002).
- Teng, B. et al. Cellular and neural responses to sour stimuli require the proton channel Otop1. *Curr. Biol.* **29**, 3647–3656 (2019).
- Teng, B. et al. Structural motifs for subtype-specific pH-sensitive gating of vertebrate otopetrin proton channels. *eLife* **11**, e77946 (2022).
- Vidavsky, N. et al. Cryo-FIB-SEM serial milling and block face imaging: large volume structural analysis of biological tissues preserved close to their native state. *J. Struct. Biol.* **196**, 487–495 (2016).

37. Bentov, S., Brownlee, C. & Erez, J. The role of seawater endocytosis in the biomineralization process in calcareous foraminifera. *Proc. Natl. Acad. Sci. USA* **106**, 21500–21504 (2009).
38. Killian, C. E. & Wilt, F. H. Endocytosis in primary mesenchyme cells during sea urchin larval skeletogenesis. *Exp. Cell Res.* **359**, 205–214 (2017).
39. Kahil, K. et al. Elemental compositions of sea urchin larval cell vesicles evaluated by cryo-STEM-EDS and cryo-SEM-EDS. *Acta Biomater.* **155**, 482–490 (2022).
40. Mann, K., Wilt, F. & Poustka, A. J. Research proteomic analysis of sea urchin (*Strongylocentrotus purpuratus*) spicule matrix. *Proteome Sci.* **8**, 33 (2010).
41. de Nooijer, L. J., Toyofuku, T. & Kitazato, H. Foraminifera promote calcification by elevating their intracellular pH. *Proc. Natl. Acad. Sci. USA* **106**, 15374–15378 (2009).
42. Dubicka, Z., Bojanowski, M. J., Bijma, J. & Bickmeyer, U. Mg-rich amorphous to Mg-low crystalline CaCO₃ pathway in foraminifera. *Heliyon* **9**, e18331 (2023).
43. Erez, J. The source of ions for biomineralization in foraminifera and their implications for paleoceanographic proxies. *Rev. Mineral. Geochem.* **54**, 15–149 (2003).
44. Harkey, M. A. & Whiteley, A. H. Isolation, culture, and differentiation of echinoid primary mesenchyme cells. *Wilhelm. Roux Arch.* **189**, 111–122 (1980).
45. Klapperstück, T. et al. Calibration procedures for the quantitative determination of membrane potential in human cells using anionic dyes. *Cytometry* **83A**, 612–626 (2013).
46. J. Warner, J. & McClay, D. R. Perturbation of the hedgehog pathway in sea urchin embryos. In *Developmental Biology of the Sea Urchin and Other Marine Invertebrates* (eds Carroll, D. J. & Stricker, S. A.) (Humana Press, New York, 2014), pp. 211–223.
47. Schewe, M. et al. A non-canonical voltage-sensing mechanism controls gating in K2P K⁺ Channels. *Cell* **5**, 937–949 (2016).
48. Petersen, I., Chang, W. J. & Hu, M. Y. Na⁺/H⁺ exchangers differentially contribute to midgut fluid sodium and proton concentration in the sea urchin larva. *J. Exp. Biol.* **224**, jeb240705 (2021).

Acknowledgements

We would like to thank R. Lingg and V. Ferfers for their help in maintaining sea urchin cultures at the Institute of Physiology at the CAU. We further thank P. Breiden for her support in preparing the constructs for heterologous expression systems. This work was supported by the European Research Council (ERC) Consolidator grant “CarboCell” Grant ID 101085894 (MYH).

Author contributions

Conceptualization: S.J., M.Y.H., M.M., T.B., C.P., M.S. Methodology: S.J., M.Y.H., T.B., M.M., M.S. Investigation: S.J., M.Y.H., C.P., M.M., M.S., O.M. Visualization: S.J., M.Y.H., C.P., M.M., M.S., O.M. Supervision: M.Y.H., M.S., T.B. Writing original draft: S.J., M.Y.H. Writing review & editing: S.J., M.Y.H., M.M., M.S., T.B., C.P., O.M.

Funding

Open Access funding enabled and organized by Projekt DEAL.

Competing interests

The authors declare no competing interests.

Additional information

Supplementary information The online version contains supplementary material available at <https://doi.org/10.1038/s41467-026-70837-x>.

Correspondence and requests for materials should be addressed to Marian Y. Hu.

Peer review information *Nature Communications* thanks Colin Brownlee and the other anonymous reviewer(s) for their contribution to the peer review of this work. A peer review file is available.

Reprints and permissions information is available at <http://www.nature.com/reprints>

Publisher's note Springer Nature remains neutral with regard to jurisdictional claims in published maps and institutional affiliations.

Open Access This article is licensed under a Creative Commons Attribution 4.0 International License, which permits use, sharing, adaptation, distribution and reproduction in any medium or format, as long as you give appropriate credit to the original author(s) and the source, provide a link to the Creative Commons licence, and indicate if changes were made. The images or other third party material in this article are included in the article's Creative Commons licence, unless indicated otherwise in a credit line to the material. If material is not included in the article's Creative Commons licence and your intended use is not permitted by statutory regulation or exceeds the permitted use, you will need to obtain permission directly from the copyright holder. To view a copy of this licence, visit <http://creativecommons.org/licenses/by/4.0/>.

© The Author(s) 2026